

## Liquid Flow through Aqueous Foams: The Node-Dominated Foam Drainage Equation

Stephan A. Koehler, Sascha Hilgenfeldt, and Howard A. Stone

*Division of Engineering and Applied Sciences, Pierce Hall, Harvard University, Cambridge, Massachusetts 02138*  
(Received 22 December 1998)

We present an experimental study of forced drainage through a soap foam, where a constant liquid flux at the top of a dry foam produces a downwards traveling wave with a constant velocity and uniform liquid content. The results are not consistent with existing models and we propose a new model, based upon relaxing the condition of wall rigidity throughout the network and emphasizing the importance of viscous damping in the nodes where Plateau borders meet. This model agrees well with the experimentally measured (power-law) scaling behavior of the drainage velocity, and the width of the propagating liquid front, on the imposed flow rate and bubble size. [S0031-9007(99)09185-1]

PACS numbers: 47.55.Mh, 82.70.Rr, 83.70.Hq

Foams are ubiquitous in everyday life and include Styro-foam, soap suds, and food (e.g., chocolate mousse and ice cream) [1,2]. Recent applications include foaming metals to make porous ultralight materials, which are useful in mechanical applications [3,4]. As with other liquid foams, metallic foams in the melt undergo *drainage*, i.e., a flow that is induced by gravity and capillarity. On a microscopic scale the liquid flow through foams is very complicated and poorly understood, even for simple aqueous foams. However, some macroscopic theories exist [5–8]. This work puts these theories to an experimental test and tries to explain the discrepancies found.

Aqueous foams consist of gas bubbles (many-sided polyhedra, *polyederschaum*) with liquid residing in the cracks between the bubbles to form a channel network. The surfactant creates a disjoining force that prevents the interfaces from rupturing and the bubbles from merging [2]. The regions between three touching bubbles are called Plateau borders, and are *channels* for liquid flow. Four channels join in the region between four touching bubbles, which we call a *node*. Figure 1 shows a network unit that consists of a node and half the lengths of the four adjoining Plateau borders. The geometry of the network is calculated using the SURFACE EVOLVER [9], which minimizes the surface energy, and results in a constant mean curvature everywhere, apart from the polyhedra's faces where the disjoining pressure dominates.

Despite the complexity of fluid flow on the level of individual channels and the complex geometry of the foam with bubbles that are in general not monodisperse, an overriding structure to fluid flow (on a scale larger than the bubble size) can be observed in many experiments, which affords a macroscopic dynamical description. We revisit here a simple experiment called forced drainage [8,10]. The primary observable is the liquid volume fraction  $\epsilon$ , the ratio of liquid volume to total volume.

The experiment starts with a column of very dry foam (typically  $\epsilon < 0.01\%$ ) in a long (170 cm) vertical tube of 2.5 cm diameter. A constant flow rate  $Q$  of liquid (identical to the foaming soap solution to minimize gradients in surfactant concentration) is introduced at the top of the

column using a syringe pump. Liquid flows downwards through the disordered channel network due to gravity. A front is observed, separating the dry foam below from the wetter foam above, which moves down with a constant velocity  $v_f$  and constant front width  $w_f$ .

A schematic of the experimental setup is shown in Fig. 2, together with a typical result for the vertical variations of  $\epsilon$  at successive times. The soap solution is composed of tap water and 0.25% Dawn soap (which is well above the critical micelle concentration), with 0.025% fluorescein salt added as a tracer. The experimental results reported here were unchanged when distilled water was used or the soap concentration was doubled or halved. The foam is generated at the lower end of the tube by a bubbler which can be exchanged to produce bubbles of different average sizes with different degrees of size dispersion (Table I). The foam is replenished by constant bubbling from the bottom, so that the “aging” (coarsening) of the foam is constant at a given height. UV light

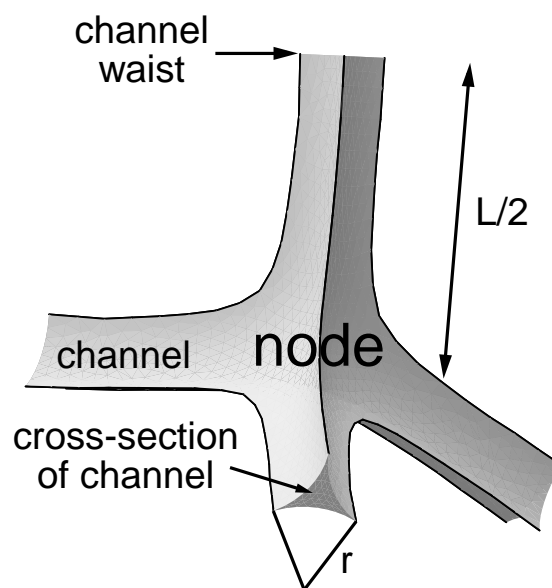


FIG. 1. Foam network unit with liquid content  $\epsilon = 0.005$ .

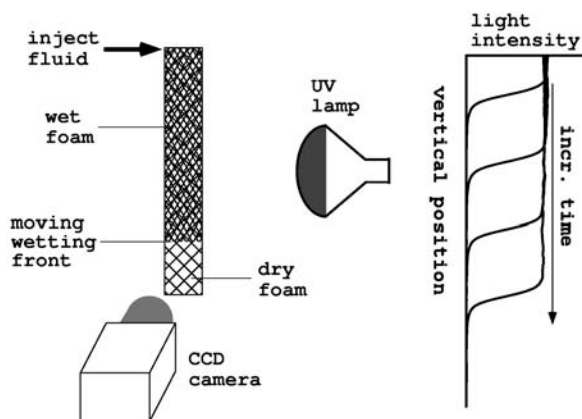


FIG. 2. Schematic of the experimental setup (left) and a typical result for the measured light intensities of the downward propagating liquid front (right).

illuminates the foam, and a CCD camera records the intensity  $I$  of the fluorescence, which is the only visible source of light in the darkened room. This allows for clean images without glaring, reflected, or scattered light. We verified experimentally that  $\epsilon \propto I$  for  $\epsilon \lesssim 0.01$ , which allows an easy way to record  $\epsilon(z, t)$ , and extract both  $v_f$  and  $w_f$ .

To eliminate the dependence of the flow rate on the cross-sectional area  $A$  of the tube, we introduce an intrinsic quantity, the *superficial velocity*  $V_s \equiv Q/A$ . Changing the tube size does not affect the results (expressed in terms of  $V_s$ ) provided that the tube diameter is much larger than  $\langle L \rangle$ , the average bubble edge length. Injecting liquid for a time  $\Delta t$  at the top produces a uniformly wetted foam behind the front spanning a volume  $v_f A \Delta t$ , thus  $\epsilon = Q \Delta t / v_f A \Delta t = V_s / v_f$ .

Figure 3 plots  $v_f$  versus  $V_s$  for three bubble sizes over about four decades of flow rate and more than two decades in  $\epsilon$  ( $5 \times 10^{-4} \lesssim \epsilon \lesssim 0.2$ ).  $v_f$  increases with  $V_s$  and bubble size, and power-law behavior of the form

$$v_f = v_0 V_s^\alpha, \quad \text{with } \alpha \approx 0.36, \quad (1)$$

is observed. The fitted prefactor  $v_0$  increases with  $\langle L \rangle$ .

Figure 4 shows the relationship between the front width  $w_f$  and  $v_f$ , determined from measuring the vertical distance between the points where the traveling profile is 20% and 80% of its maximum height, respectively. The front narrows with increasing  $V_s$  and decreasing  $\langle L \rangle$ . There is an approximately inverse relationship between  $w_f$  and  $v_f$ ,

$$w_f = w_0 v_f^\beta, \quad \text{with } \beta \approx -0.95. \quad (2)$$

Experiments show that at higher  $\epsilon$  (higher  $v_f$  than in Fig. 4) the data for front width versus  $v_f$  levels off.

TABLE I. Bubbling equipment, bubble average polyhedral edge length  $\langle L \rangle$ , and relative standard deviation of  $\langle L \rangle$ .

| Bubble size | Bubbler                  | $\langle L \rangle$ (cm) | $\frac{\sigma(L)}{\langle L \rangle}$ |
|-------------|--------------------------|--------------------------|---------------------------------------|
| Large       | 0.2 mm capillary tube    | 0.20                     | 0.235                                 |
| Medium      | Extra-coarse glass frits | 0.083                    | 0.309                                 |
| Small       | Coarse glass frits       | 0.051                    | 0.324                                 |

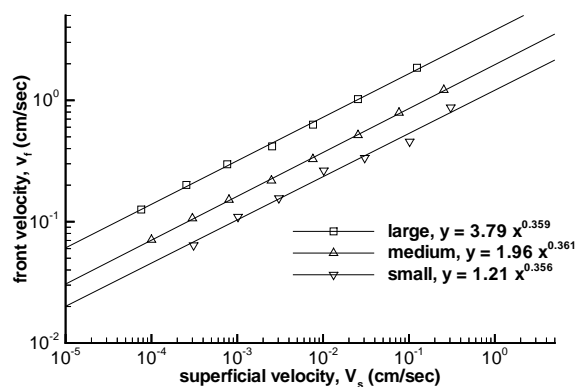


FIG. 3. Front velocity as a function of superficial velocity for three different bubble sizes. Solid lines are best fits.

To model forced drainage, we consider low flow rates and small capillary numbers  $\mu v_f / \gamma \ll 1$ , with fluid viscosity  $\mu$  and surface tension  $\gamma$ , so that the capillary forces are large compared with the stresses that may distort the foam. Thus, the geometry of the idealized gravity-free, zero-flux foam (Fig. 1) should be essentially preserved in the experiment, which is confirmed by visual observation.

In the dry limit, the channels are to a good approximation straight, slender units whose lengths approach  $L$  (see Fig. 1) with a transverse radius of curvature  $r$  at their waist. The volume of one channel is  $aL$ , where the cross-sectional area is  $a = \delta_a r^2$ , with  $\delta_a = (\sqrt{3} - \pi/2) \approx 0.1613$  [8]. The node volume is  $\mathcal{O}(r^3)$ , as the node size is proportional to  $r$ , and is negligible compared to the channel volume. Thus the volume of a liquid network unit is  $2aL$ . We assume that the foam is composed of monodisperse tetrakaidecahedra (Kelvin cells), mimicking the polyhedral bubbles found in a real foam [11]. Each tetrakaidecahedron has 12 complete channels, 6 complete nodes, and volume  $\delta_{\text{vol}} L^3$  with  $\delta_{\text{vol}} = 2^{7/2}$ . For low volume fractions  $\epsilon \lesssim 0.10$ ,

$$\epsilon \approx \delta_\epsilon r^2 / L^2 \quad \text{with } \delta_\epsilon = 12 \delta_a / \delta_{\text{vol}} \approx 0.1711. \quad (3)$$

Above this, the channels are no longer long and slender, the nodes contain an appreciable part of the liquid, and a simple theory is far more difficult to develop.

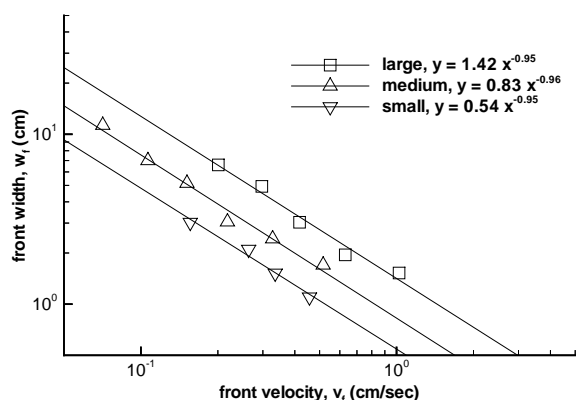


FIG. 4. Front width as a function of front velocity for three different bubble sizes. Solid lines are best fits.

To model the power-law behaviors (1) and (2) involving  $v_f$  and  $V_s$ , it is necessary to obtain a relation between  $v_f$  and  $\epsilon$  (or  $r$ ) which, with  $\epsilon = V_s/v_f$ , closes the system of equations. In general,  $v_f(\epsilon)$  can be determined from the Navier-Stokes equations, although a first-principle calculation is well beyond the scope of this investigation.

We first discuss the main body of the traveling wave, where redistribution of liquid among the channels due to capillarity leads to a constant  $\epsilon$  (see Fig. 2). The structure is periodic from channel to channel, and there are no pressure gradients on a macroscopic scale, which ensures that all channels have the same  $r$  *regardless of orientation* [8]. Since the velocity field is time independent and the Reynolds numbers are small [ $\mathcal{O}(0.01-10)$ ], a volume integral of the Stokes equation over many bubbles yields

$$\int_{\mathcal{V}_{\text{liq}}} (\nabla p - \rho \mathbf{g}) d\mathcal{V} = \int_{\mathcal{V}_n} \mu \nabla^2 \mathbf{u} d\mathcal{V} + \int_{\mathcal{V}_c} \mu \nabla^2 \mathbf{u} d\mathcal{V}, \quad (4)$$

where the liquid volume  $\mathcal{V}_{\text{liq}}$  is divided among channels  $\mathcal{V}_c$  and nodes  $\mathcal{V}_n$ , and the microscopic liquid velocity is denoted by  $\mathbf{u}$ . The first integral is the driving force, the second and third are the damping forces in the nodes and the channels, respectively. Because of the periodicity the integral over  $\nabla p$  vanishes away from the front region.

Traditionally, models assume *rigid walls* throughout the whole network [6,7,12,13]. Then, since the channels have a cross section smaller than, and a length longer than, the nodes, the third integral of (4) dominates the second term. The flow then resembles gravity-driven Poiseuille pipe flow. For a given channel orientation  $\hat{\mathbf{s}}_i$  and flow rate  $q_i$  we have  $\rho \mathbf{g} \cdot \hat{\mathbf{s}}_i \approx \mu \delta_\mu q_i / a^2$ , where  $\delta_\mu$  depends on the geometry of the cross-sectional area. For the curved Plateau borders  $\delta_\mu \approx 50$  [8].

Let  $N$  be the typical number of channels in the tube's cross-section. The front velocity is the average vertical liquid velocity

$$v_f = \frac{1}{N} \sum_{i=1}^N \frac{q_i}{a} \hat{\mathbf{s}}_i \cdot \hat{\mathbf{z}} = \frac{a \rho g}{N \delta_\mu \mu} \sum_{i=1}^N (\hat{\mathbf{s}}_i \cdot \hat{\mathbf{z}})^2 = \frac{\delta_a r^2 \rho g}{3 \delta_\mu \mu}, \quad (5)$$

where Poiseuille flow is assumed and the last equality (the factor of three) follows from the random orientation of channels. In the limit of dry foams, using (3), (5), and  $\epsilon = V_s/v_f$ , we get

$$v_f = (V_0^{\text{rigid}} V_s)^{1/2}, \quad \text{where } V_0^{\text{rigid}} = \frac{\delta_a \rho g L^2}{3 \delta_\epsilon \delta_\mu \mu}. \quad (6)$$

This assumption of rigid channel walls predicts an exponent  $\alpha = 1/2$  for (1), as reported earlier [10,12,13], which is in disagreement with the data presented here (Fig. 3). Nor does a variation of this model [8] which introduces a surface viscosity due to the presence of sur-

factants produce the power-law behavior we observe. We therefore question the assumption of rigid channel walls, and propose an alternative approach in which the channel's surface has slip (small stresses at the boundaries; cf. [5,14]). Assuming that the flow in the channels is pluglike, the damping force of the third integral in (4) is small. However, in the nodes, flows from different channels merge and give rise to velocity gradients on a length scale  $r$ , thereby dominating viscous damping.

The second integral in (4) can be rewritten by removing the length scale  $r$ , and the velocity scale  $\mathbf{v}$ , which here has magnitude equal to the front velocity  $v_f$ ,

$$\int_{\mathcal{V}_n} \mu \nabla^2 \mathbf{u} d\mathcal{V} = -n I r \mu \mathbf{v}, \quad (7)$$

$$I \equiv \left| \frac{1}{n} \int_{\tilde{\mathcal{V}}_n} \tilde{\nabla}^2 \tilde{\mathbf{u}} d\tilde{\mathcal{V}} \right|,$$

where  $n$  is the number of nodes in  $\mathcal{V}_n$  and  $\tilde{\cdot}$  denotes dimensionless quantities.  $I$  is a dimensionless number representative of the viscous force in the nodes assumed to be independent of  $\epsilon$ . Dividing (4) by  $2naL$ , the foam liquid volume containing  $n$  nodes, and using (3) and (7), gives

$$-\nabla p_{\text{macro}} + \rho \mathbf{g} = \frac{\mu \mathbf{v}}{\kappa(\epsilon)}, \quad \text{where } \kappa(\epsilon) = \frac{2 \delta_a L^2 \epsilon^{1/2}}{\delta_\epsilon^{1/2} I}. \quad (8)$$

Here the macroscopic pressure gradient  $\nabla p_{\text{macro}}$  is defined as the derivative of  $p$  on a macroscopic scale, with all variations on a scale smaller than  $L$  averaged out. Equation (8) is a form of Darcy's equation for flow through porous media with a permeability  $\kappa(\epsilon)$ . In contrast, the channel-dominated flow model yields a permeability  $\kappa(\epsilon) \propto L^2 \epsilon$ .

In the main body of forced drainage, there are no macroscopic pressure variations, and using (8) we obtain

$$v_f = [(V_0^{\text{slip}})^2 V_s]^{1/3}, \quad \text{where } V_0^{\text{slip}} = \frac{2 \delta_a \rho g L^2}{\mu \delta_\epsilon^{1/2} I}, \quad (9)$$

i.e., an exponent  $\alpha = 1/3$  which is about 8% lower than the measured exponents. Several effects could contribute to a deviation from a 1/3-power law, e.g., (i) for narrow tubes, whose diameter is only a few bubble diameters, the rigid tube walls should play a greater role providing dissipation. Indeed, for experiments with a tube of 0.6 cm diameter and  $\langle L \rangle = 0.2$  cm,  $\alpha$  increases about 20%. (ii) Contributions to dissipation from small viscous stresses in the channels would also tend to increase  $\alpha$ , cf. (6). See Table II for a comparison between the measurements and model predictions.

Now we discuss the front shape and width. The Young-Laplace law for pressure drop across liquid-air interfaces yields in the dry foam limit  $\Delta p = p_{\text{gas}} - p \approx \gamma/r$ , at the channel's waist (Fig. 1). For low flow rates, the gas pressure inside the bubbles will not change appreciably. Thus averaging  $p$  gives the macroscopic pressure gradient  $\nabla p_{\text{macro}} \approx -\gamma \nabla r^{-1}$ .

TABLE II. Experimental data for the exponents  $\alpha$  and  $\beta$  and the prefactor  $w_0$  of Eqs. (1) and (2). Also shown are the relative errors in the predictions for  $\alpha$  and  $\beta$  from the rigid-channel theory and the channel-slip theory presented here. As  $\beta$  is close to the experimental value only for the channel-slip theory, the relative error of  $w_0$  is given only for this case, see (12).

| Size   | $\alpha$ |       |      | $\beta$ |       |      | $w_0$ |      |
|--------|----------|-------|------|---------|-------|------|-------|------|
|        | Expt.    | Rigid | Slip | Expt.   | Rigid | Slip | Expt. | Slip |
| Large  | 0.359    | 40%   | 7%   | -0.95   | 47%   | 5%   | 1.42  | 51%  |
| Medium | 0.361    | 39%   | 8%   | -0.96   | 48%   | 4%   | 0.83  | 20%  |
| Small  | 0.356    | 40%   | 6%   | -0.95   | 47%   | 5%   | 0.54  | 3%   |

To obtain a dynamical equation for the macroscopic quantity  $\epsilon$ , we start with the volume conservation equation for the liquid,  $\partial\epsilon/\partial t + \nabla \cdot (\mathbf{v}\epsilon) = 0$ . Eliminating  $r$  using (3) from  $\nabla p_{\text{macro}}$  and substituting into (8) to obtain  $\mathbf{v}$  yields the node-dominated foam drainage equation:

$$\frac{\mu \delta_\epsilon^{1/2} I}{2\delta_a L^2} \frac{\partial \epsilon}{\partial t} + \rho \mathbf{g} \cdot \nabla \epsilon^{3/2} - \frac{\gamma \delta_\epsilon^{1/2}}{2L} \nabla^2 \epsilon = 0. \quad (10)$$

The 1D dimensionless form appropriate here, projecting onto  $\hat{\mathbf{z}}$ , is  $\partial_\tau \epsilon - \partial_\zeta \epsilon^{3/2} - \partial_\zeta^2 \epsilon = 0$  with length scale  $(\delta_\epsilon^{1/2} \gamma)/(2\rho g L)$  and time scale  $\delta_\epsilon I \gamma \mu / 4\delta_a \rho^2 g^2 L^3$ .

For forced drainage, the ansatz  $\epsilon(\zeta, \tau) = f(\zeta + v\tau) = f(s)$  transforms to the reference frame of the wave traveling at the nondimensional speed  $v$  of liquid drainage. The resulting ordinary differential equations can be solved analytically and the  $\epsilon$  profile is the square of a Fermi function,

$$f(s) = \frac{v^2}{[1 + e^{\nu(s_0-s)/2}]^2}, \quad (11)$$

where  $s_0$  sets the front position in the traveling frame  $s$ . Here, the width of the front, using the experimental 80% to 20% criterion, is  $\Delta s \approx 4.70/v$ , or with dimensions

$$w_f = 2.35 \frac{\delta_\epsilon^{1/2} \gamma}{\rho g L} \frac{V_0^{\text{slip}}}{v_f} \approx 0.020 \frac{V_0^{\text{slip}}}{v_f} \frac{\text{cm}^2}{L} \quad (12)$$

using  $\gamma \approx 20$  g/sec<sup>2</sup> for soapy water. Equation (9) shows  $V_0^{\text{slip}} \propto L^2$ , so  $w_f$  in (12) increases linearly with  $L$ , which is the trend seen in Fig. 4.

The rigid channel model yields a different front width [6]. Using the 80% to 20% criterion, we find  $w_f = 0.556 \gamma \delta_a^{1/2} (\delta_\mu \rho g \mu)^{-1/2} v_f^{-1/2}$  with the predicted exponent  $\beta = -1/2$ , rather than the measured  $\beta \approx -1$ . This model also predicts that the front width does *not* vary with bubble size, whereas experiments show that  $w_f$  increases with  $\langle L \rangle$ .

It is possible to estimate the prefactor for  $w_f$  in (2) from (12), given  $V_0^{\text{slip}} = v_0^{3/2}$  from (1) and (9), with  $v_0$  determined from the best-fit lines of Fig. 4. We point out, however, that our analysis was based upon monodisperse uniform foams, whereas in the experiments there are size variations of about 30%. Table II summarizes the relative differences between the experimentally determined expo-

nents  $\alpha$ ,  $\beta$ , and those from the two models, rigid wall (channel dominated) and slip (node dominated).

The forced drainage experiments presented here show robust power-law behavior for the dependence of front velocity on superficial velocity,  $v_f \propto V_s^\alpha$  with  $\alpha \approx 1/3$ , over several decades of flow rates and for different bubble sizes. Furthermore  $w_f \propto V_s^\beta$  with  $\beta \approx -1$ , and the proportionality factor increases with bubble size. These results suggest that at least for a certain class of surfactants the no-slip assumption is invalid. A simple new model based upon slipping walls and dissipation in the nodes for the regime of dry monodisperse foams does much better predicting both  $\alpha$  and  $\beta$ , and also has the correct trend of front width increasing with bubble size.

We thank A. Evans for support of this project, A. Kraynik for his help with the Surface Evolver and useful suggestions, as well as J. Eggers and J. Sherwood for helpful discussions. Support from ONR Grant No. N00014-1-96-1028 is gratefully acknowledged.

- [1] J.J. Bikerman, *Foams* (Springer, New York, 1973).
- [2] *Foams*, edited by R.K. Prud'homme and S.A. Khan (Marcel Dekker, New York, 1996).
- [3] L.J. Gibson and M.F. Ashby, *Cellular Solids* (Cambridge University Press, Cambridge, 1997).
- [4] A.G. Evans, J.W. Hutchinson, and M.F. Ashby, *Curr. Opin. Solid State Mater. Sci.* **3**, 288 (1998).
- [5] A.M. Kraynik, Sandia National Laboratories Report No. 83-0844, 1983.
- [6] D. Weaire, S. Hutzler, G. Verbist, and E. Peters, *Adv. Chem. Phys.* **102**, 315 (1997).
- [7] A. Bhakta and E. Ruckenstein, *Adv. Colloid Interface Sci.* **70**, 1 (1997).
- [8] R.A. Leonard and R. Lemlich, *AIChE J.* **11**, 18 (1965).
- [9] University Minnesota Geometry Center, Surface Evolver Version 2.10c; <http://www.geom.umn.edu>, 1998.
- [10] D. Weaire, N. Pittet, S. Hutzler, and D. Pardal, *Phys. Rev. Lett.* **71**, 2670 (1993).
- [11] H.M. Princen, *Langmuir* **2**, 519 (1986).
- [12] I.I. Goldfarb, K.B. Kann, and I.R. Shreiber, *Fluid Dyn.* **23**, 244 (1988).
- [13] G. Verbist, D. Weaire, and A. Kraynik, *J. Phys. Condens. Matter* **8**, 3715 (1996).
- [14] D. Desai and R. Kumar, *Chem. Eng. Sci.* **37**, 1361 (1982).